LAWRENCE
LIVERMORE
NATIONAL
LABORATORY

LLNL-JRNL-654005

Generation and Focusing of Electron Beams with Initial Transverse-Longitudinal Correlation

J. R. Harris, J. W. Lewellen, B. R. Poole

May 5, 2014

Journal Of Applied Physics

Disclaimer

Generation and Focusing of Electron Beams with Initial Transverse-Longitudinal Correlation

J.R. Harris*

Department of Electrical and Computer Engineering,
Colorado State University, Fort Collins, CO 80523

J.W. Lewellen

Los Alamos National Laboratory, Los Alamos, NM 87545

B.R. Poole

Lawrence Livermore National Laboratory, Livermore, CA 94550

ABSTRACT

In charged particle beams, one of the roles played by space charge is to couple the transverse and longitudinal dynamics of the beam. This can lead to very complex phenomena which are generally studied using computer simulations. However, in some cases models based on phenomenological or analytic approximations can provide valuable insight into the system behavior. In this paper, we employ such approximations to investigate the conditions under which all the slices of a space charge dominated electron beam with slowly-varying current could be focused to a waist with the same radius and at the same location, independent of slice current, and show that this can be accomplished approximately if the initial transverse-longitudinal correlation introduced onto the beam by the electron gun is chosen to compensate for the transverse-longitudinal correlation introduced onto the beam in the drift section. The validity of our approximations is assessed by use of progressively more realistic calculations. We also consider several design elements of electron guns that affect the initial correlations in the beams they generate.

* Electronic mail: john.harris@colostate.edu.

I. Introduction

In charged particle beams, space charge couples the transverse and longitudinal dynamics of the beam, so that longitudinal variation in the beam's current leads to different rates of radial expansion along its length. One well-known result of this is the growth in the projected emittance of the beam, which occurs when space charge causes different regions of the beam to evolve differently in phase space, so that the area occupied by the entire beam in phase space increases significantly, even though the emittance of each slice of the beam remains unchanged. Projected emittance growth motivated the development of emittance compensation [1,2], which is of particular importance in photoinjectors and other short pulse machines. However, the need to properly handle the effects of space charge is not limited to photoinjectors. Techniques to deal with this coupling must be employed in any machine where space charge is significant and the loss of particles from the lower-current regions of the beam cannot be accepted. This is particularly true in machines where the beam is generated with a significant initial transverse-longitudinal correlation [3,4] and must be transported through a channel while avoiding beam loss and heating of metallic structures [5] or charging and breakdown of dielectric-lined structures [6,7] placed in close proximity to the beam edge. While these effects can be very complicated and are generally investigated using computer simulations, having design tools or scaling relations based on phenomenological or analytic approximations can be of great value in understanding the design trade space. Such relations are often easily developed for idealized beam transport systems, but they are of limited value unless they also incorporate the transverse-longitudinal correlation generated in the gun and injection region, which determines the initial conditions of the beam on injection into that transport system. Alternatively, those simple models could be used if the injection region itself were designed in such a way as to remove the

initial transverse-longitudinal correlation, for example by throwing each slice of the beam to a waist with radius and location which is independent of slice current. The beam could then be handed off to the downstream transport system with an initial radius and divergence which are independent of slice current, and therefore amenable to simple approximate models for the transport system itself.

To develop such a model, we must first choose an injector architecture; the simplest architecture in widespread use is that of an electron gun immediately followed by a solenoid lens and drift section (Figure 1). We next require simplified, analytically-tractable models for each of the three elements. For the electron gun itself, simulations indicate that low voltage electron guns operating in the DC limit produce beams with initial radii and divergences that can be expressed to good approximation as linear functions of beam current, with the coefficients depending on the gun geometry [3,4], while the solenoid can easily be approximated as a thin lens. For the drift section, as shown in Figure 1 where each slice is thrown to a waist at a common location, we simply need a model for beam expansion from a waist. While the well-known quadratic model for expansion of a cold beam is often used [8], we will instead use a more complicated model, introduced in Ref. [9], which produces reasonable accuracy over a wider range of beam radii.

Our approach is to combine these three models to describe the evolution of each slice of the beam. Each of these models incorporates assumptions which will be described in detail. However, the fundamental assumption is that every slice of the beam can be treated independently of every other slice. This implies that there is no longitudinal evolution of the beam, and a variation in current which is slow compared to the transit time across the diode. Beams with large, slow variation in current but negligible variation in energy, as assumed here,

can be achieved in DC guns where the emission current is being modulated, rather than the anode-cathode voltage. This modulation can be accomplished in a number of ways, including the use of a gridded cathode [7] or gated field emission arrays [11,12], or by using a long-pulse laser to photomodulate the beam from a thermionic cathode [13,14]. Such deliberate current modulation might be used, for example, to introduce a seed signal onto the beam for interaction with a slow wave structure in a high power microwave source [7]. Current modulation is also likely to occur in guns using flashboard plasma cathodes due to changes in the gun perveance caused by the expansion of the plasma across the anode-cathode gap [15,16,17], unless a sufficiently short extraction voltage pulse is used [18]. Finally, slow changes in beam current could also occur in high power machines due to back-bombardment and subsequent heating of a thermionic cathode by ions or electrons. And while electron back-bombardment is primarily of concern in RF guns [19], the approach discussed here could be of use to the designers of systems using those guns if their primary concern was minimizing changes in the beam spot size associated with a slice of the beam extracted at a particular RF phase caused by cathode temperature changes occurring much slower than the RF period.

Our objectives in this paper are therefore twofold: first, from a theoretical standpoint, to combine the simple models discussed above and assess the validity of the resulting overall model; and second, from a practical standpoint, to develop a simple design tool for high current injectors. We begin by assembling our simplified models, working backward from the waist, in order to establish requirements on the electron gun, and noting along the way various limitations on those models. We then compare the full model to a sample configuration, again looking to validate its utility. Finally, we will consider the role played by electron gun design in

establishing the beam's initial transverse-longitudinal correlation, identifying design elements that could enable generation of the initial beam configuration required by our model.

II. Model Development and Limitations.

A. Drift Section

1. Model

Our first step is to consider the beam evolution between the lens and waist. Because of the time-reversibility of the envelope equation, the envelope will be symmetric about the waist, and so we can use our approximation for the expansion of a cold beam from a waist of radius r_w, introduced in Ref. [9], to model the compression of a beam slice with current I:

$$r_b(z) \approx r_w + 0.303 r_w^{-0.617} \left[\sqrt{\frac{4I}{I_0 \beta^3 \gamma^3}} \right]^{1.617} z^{1.617} . \quad (1)$$

Here β and γ are the relativistic factors, I_0 is the characteristic current (17kA for electrons), and z is the magnitude of the displacement away from the waist. The beam divergence is then

$$r_b'(z) \approx -1.617 \times 0.303 r_w^{-0.617} \left[\sqrt{\frac{4I}{I_0 \beta^3 \gamma^3}} \right]^{1.617} z^{0.617} , \quad (2)$$

with the minus sign used here because the beam is undergoing radial compression, rather than expansion. The radius and divergence of the beam are related at any location by

$$r_b' \approx \frac{1.617}{z} \left(r_w - r_b \right) , \quad (3)$$

which defines a line in trace space along which the beam radius and divergence for each slice of the beam must lie (Figure 2). Only part of this line will be populated, bounded on one side by the radius and divergence of the highest-current slice of the beam (point A), and on the other by

the radius and divergence of the lowest-current slice of the beam (point B). If the beam current varies from zero to $I_{\max}$, point A will be given by

$$\left(r_w + 0.303 r_w^{-0.617} \left[\sqrt{\frac{4I_{\max}}{I_0 \beta^3 \gamma^3}} \right]^{1.617} z^{1.617}, -1.617 \times 0.303 r_w^{-0.617} \left[\sqrt{\frac{4I_{\max}}{I_0 \beta^3 \gamma^3}} \right]^{1.617} z^{0.617} \right), \quad (4)$$

while point B will be given by

$$(r_w, 0). \quad (5)$$

2. Limitations

This model makes two primary physical assumptions. The first, mentioned earlier, is that every slice of the beam evolves independently of every other slice, so that there is no longitudinal evolution in the beam. Longitudinal evolution in beams typically occurs much more slowly than transverse evolution, but very rapid changes in beam current can generate space charge waves leading to significant changes in the longitudinal pulse shape, interference effects [20], and other complicated behavior in convergent beams injected into transport channels [21], none of which is incorporated into our model.

Second, the model assumes a zero-emittance beam. Zero-emittance beams are a theoretical abstraction, but a useful one, and within this assumption the model provides reasonably good accuracy; when calculating the envelope of a beam launched from a waist, the maximum error between Eq. (1) and a direct integration of the envelope equation is about 5%, while the average error is about 2% over the range $r_w \le r \le 6.6 r_w$ [9]. All other things being equal, space charge becomes a relatively more important factor as beam radii become larger, while emittance becomes a relatively more important factor as beam radii become smaller. Therefore, our assumption should be acceptable as long as the emittance-limited spot size is

much smaller than the actual beam waist. The beam envelope in the absence of space charge and focusing is [8]

$$r(z) = \left[r_0^2 + 2r_0 r_0' z + \left(\frac{\varepsilon^2}{r_0^2} + r_0'^2 \right) z^2 \right]^{1/2}, \tag{6}$$

where r_0 is the initial radius, r_0' is the initial divergence, ε is the emittance, and z is the distance along the direction of propagation; this implies an emittance-limited waist radius of

$$r_{w,\varepsilon} = \left[r_0^2 - \frac{\left(r_0 r_0' \right)^2}{\left(\frac{\varepsilon^2}{r_0^2} + r_0'^2 \right)} \right]^{1/2}. \tag{7}$$

As an example, Figure 3 shows the case of a 100 mA, 50 keV beam with initial radius of 2.969 mm and divergence of -0.016, predicted by Eqs. (1) and (2) to give a waist of 1 mm at a location 20 cm downstream. The black curve is given by Eq. (1), while the blue, gray, red, and green curves are from numerical integration of the envelope equation [8]

$$r'' + k_0^2(z) r - \frac{2I}{I_0 \beta^3 \gamma^3 r} - \frac{\varepsilon^2}{r^3} = 0, \tag{8}$$

where the primes denote differentiation with respect to z, k_0^2 defines the external focusing strength (which is zero for this calculation but will be used later), and assuming emittance values of zero, 4.02 μm, 8.12 μm, and 17.00 μm, corresponding to emittance-limited waist sizes found from Eq. (7) of 0, 0.25 mm, 0.5 mm, and 1 mm respectively. These curves confirm the validity of our assumption that when the emittance-limited waist size is much smaller than the actual waist, our model for beam transport in a drift is reasonably accurate.

B. Beam Configuration Upstream of the Thin Lens

Immediately downstream of the lens, the beam must have the radius $r_b(I)$ and divergence $r_b'(I)$ given by Eqs. (1) and (2). Immediately upstream of the lens, the radius must therefore be

$$r_a(I) = r_b(I) = r_w + 0.303 r_w^{-0.617} \left(\sqrt{\frac{4I}{I_0 \beta^3 \gamma^3}} \right)^{1.617} z_w^{1.617} \tag{9}$$

and the divergence must be

$$r_a'(I) = r_w k_0^{\,2} L + 0.303 \left(k_0^{\,2} L - \frac{1.617}{z_w} \right) r_w^{-0.617} \left(\sqrt{\frac{4I}{I_0 \beta^3 \gamma^3}} \right)^{1.617} z_w^{1.617} . \tag{10}$$

Eqs. (9) and (10) again define a line in trace space,

$$r_a' = r_a \left(k_0^2 L - \frac{1.617}{z_w} \right) + r_w \frac{1.617}{z_w}, \tag{11}$$

along which the beam slices lie (Figure 4). We can again define two key points corresponding to those shown in Figure 2. The point B, associated with the zero-current slice of the beam, will be at

$$(r_w, r_w k_0^2 L), \tag{12}$$

and the point A, associated with the peak-current slice of the beam, will be at

$$\left(r_w + 0.303 r_w^{-0.617} \left[\sqrt{\frac{4I_{\max}}{I_0 \beta^3 \gamma^3}} \right]^{1.617} z_w^{\,1.617}, \right.$$

$$\left. r_w k_0^2 L + 0.303 \left(k_0^2 L - \frac{1.617}{z_w} \right) r_w^{-0.617} \left[\sqrt{\frac{4I_{\max}}{I_0 \beta^3 \gamma^3}} \right]^{1.617} z_w^{\,1.617} \right). \tag{13}$$

C. Electron Gun

1. Model

We next consider the electron gun itself. The space charge driven transverse-longitudinal correlation occurring in DC guns can be viewed as the result of the competition between the

time-independent focusing forces in the gun and the time-dependent transverse space charge forces in the beam. Simulations of low-voltage electron guns employing electrostatic focusing show that the beam radius and divergence at the anode can be approximated very well as linear functions of the beam current, with the coefficients of the linear fitting functions depending on the gun geometry [3]. This provides a convenient way to parameterize the beam's radius and divergence at the gun exit. At that location, the radius r and divergence r' of each slice of the beam would depend on the beam current I according to

$$r = a_0 + a_1 I \tag{14}$$

and

$$r' = b_0 + b_1 I \,. \tag{15}$$

The beam radius and divergence are then related by

$$r' = \left(\frac{b_1}{a_1} \right) r + \left(b_0 - \frac{a_0 b_1}{a_1} \right), \tag{16}$$

which defines a line in trace space along which the radius and divergence of the beam edge for each slice of the beam must lie (Figure 5). This line is populated between a point B defined by

$$\left(a_0, b_0 \right) \tag{17}$$

corresponding to the zero-current slice of the beam, and a point A defined by

$$\left(a_0 + a_1 I_{\max}, b_0 + b_1 I_{\max} \right) \tag{18}$$

corresponding to the peak-current slice of the beam containing a current $I_{\max}$.

2. Limitations.

The linear parameterization of initial beam radius and divergence employed here was introduced in Ref. [4] based on electron gun simulations reported in Ref. [3]. In those simulations, performed using the codes CST Particle Studio [22], SPIFFE [23], and TRAK [24],

DC electron guns having a variety of anode-cathode spacings, voltages, and focusing electrode angles were operated at a series of currents from "zero current" to the space charge limit. No beam extraction aperture was included, both to replicate guns where an anode grid is used [25,26], and to avoid complications associated with beam scraping and particle loss during transmission through the aperture [27]. Figure 6 shows a typical example of one of these simulations, using an anode-cathode spacing of 25 mm, emission surface radius of 4 mm, and a focusing electrode angle of 100° rather than the typical 67.5° Pierce angle [28]. This angle causes the beam arriving at the anode to be diverging at all currents; although unusual, guns designed to deliberately defocus the beam in the diode region have been employed in special roles, such as the original injector for the FXR linear accelerator at Lawrence Livermore National Laboratory [25]. The trace space diagram shows the results of 17 runs at currents between 0.1 mA ("zero current," B) and 1.33 A (the space charge limited current, A); note that these points fall along the line defined by Eq. (16), indicating excellent agreement between the simulation results and the inferred linear parameterization.

As the previous simulations were performed at nonrelativistic voltages between 0.5 kV and 20 kV, a valid question is whether a linear parameterization is also useful for higher energy guns, and guns without anode grids. For these purposes, we limit ourselves to voltages of 500 kV and lower; at voltages higher than this, the problems of preventing electrical breakdown in both DC and pulsed electron guns become very challenging, and the design of insulating structures to control these breakdown processes, particularly vacuum surface flashover [29] remains an active area of research [30,31,32]. Accordingly, new simulations were performed of apertured electron guns at 100 kV, 300 kV, and 500 kV using the code TRAK [24], as shown in Figure 7. In all cases, the focusing electrode angle was 67.5°, cathode radius was 0.5 cm, anode

aperture radius was 0.6 cm, and anode-cathode distance was 3 cm. One diagnostics plane was placed in the plane of the aperture, and three more were placed 0.6 cm, 1.2 cm, and 1.8 cm downstream of the aperture plane. Data was extracted by taking the beam edge radius and divergence directly from the phase space data, as well as two different statistical methods. Figure 8 shows the beam radius and divergence at the four diagnostic locations for the gun at 500 kV using data extracted directly from the phase space plots generated by the simulation, compared to linear fitting functions for each case. This combination of voltage and data extraction method actually generated the *least linear* results of all the nine combinations tried. While there is some curvature in the data, suggesting that a quadratic fit would yield a closer result, it is also clear that the linear approximation for beam radius and divergence as a function of beam current remains useful even for apertured guns with voltages entering the relativistic regime [33].

We will return to a discussion of electron gun design, and the impact of their design on transverse-longitudinal correlations introduced in the gun, in Section IV.

D. Matching of Electron Source and Transport Channel

To complete the model, note that the trace space configurations shown in Figures 4 and 5 have been deliberately drawn to share the same general shape. In order to approximately match the desired trace space configuration defined by Eqs. (9) and (10) to the type of trace space configuration we expect from electron guns as defined by Eqs. (14) and (15), we can simply associate the zero-current endpoints B and the peak-current endpoints A in the two figures. Equating Eq. (12) with Eq. (17), and Eq. (13) with Eq. (15), yields the conditions

$$a_0 = r_w , \tag{18}$$

$$a_1 = 0.303 r_w^{-0.617} \left(\frac{4}{I_0 \beta^3 \gamma^3} \right)^{\frac{1.617}{2}} z_w^{1.617} I_{\max}^{\frac{1.617}{2}-1}, \tag{19}$$

$$b_0 = r_w k_0^{\,2} L, \tag{20}$$

and

$$b_1 = 0.303 \left(k_0^{\,2} L - \frac{1.617}{z_w} \right) r_w^{-0.617} \left(\frac{4}{I_0 \beta^3 \gamma^3} \right)^{\frac{1.617}{2}} z_w^{1.617} I_{\max}^{\frac{1.617}{2}-1}. \tag{21}$$

These coefficients define an *approximate linear parameterization* of the desired initial conditions, using the form of Eqs. (14) and (15). We must emphasize that this is only an approximate parameterization, which holds exactly for the peak- and zero-current slices only. Use of these parameters with Eqs. (14) and (15) will effectively distribute the intermediate slices between the peak- and zero-current slices as if they had a linear dependence on current, instead of the actual $I^{1.617/2}$ dependence required by Eqs. (9) and (10). Thus while Eqs. (18) - (21) replicate the trace space geometry of the desired initial beam, they incorrectly replicate the "internal configuration" of the beam within that area in trace space. Despite this, since the bounding peak-current and zero-current cases are treated correctly, it is reasonable to think that this approximate approach may still work relatively well.

It is also interesting to note the limitations imposed on possible solutions by Eqs. (18) - (21). First, the waist radius is constrained by Eq. (18). The a_n and b_n parameters depend solely on the gun geometry and voltage, and so must be constants, and therefore Eq. (18) indicates that r_w must also be independent of beam current or solenoid focusing strength. This is because there is no space charge in the zero current slice to drive radial expansion, so its radius at the waist and its radius on leaving the lens must be the same [34]. And since we have assumed a thin lens, the

radius of the zero current slice will not change while passing through the lens, forcing $r_w = a_0$, and implying r_w to be a constant defined by the gun geometry and which must be the same for every slice of the beam.

Second, Eq. (20) implies that the lens strength $k_0^2 L$ is defined by the ratio of the zero-current beam radius and divergence produced by the gun. This is because one function of the lens is to adjust the divergence of the zero current beam. And since $k_0^2 L \geq 0$ for a solenoid, Eq. (20) also implies that the zero-current slice of the beam must be initially diverging $(b_0 \geq 0)$. This is a condition not normally found in electron guns, which are more typically designed to produce converging beams or rectilinear flow at full current [28], and therefore are converging at low current.

Similarly, Eqs. (19) and (21) imply that z_w and $I_{\max}$ may also take on a single value; for z_w this is

$$z_w = \frac{1.617}{\frac{b_0}{a_0} - \frac{b_1}{a_1}}, \tag{22}$$

and for $I_{\max}$ this is

$$I_{\max} = \left[\frac{a_1 a_0^{\,0.617} \left(\frac{b_0}{a_0} - \frac{b_1}{a_1} \right)^{1.617}}{1.617^{1.617} \times 0.303 \left[\sqrt{\frac{4}{I_0 \beta^3 \gamma^3}} \right]^{1.617}} \right]^{-5.22}. \tag{23}$$

Thus, specifying the gun design specifies all other system parameters.

III. Example Case

A. Applying the Model

To study the validity of our models, we now use them to consider an example case. We begin by computing the required electron gun parameters, and then progressively relaxing our assumptions. We consider a beam of energy 75 keV, whose current varies from 0 to 1 A, generated in an electron gun using a thermionic cathode of radius r_k = 5 mm operating at a temperature of T = 800 K. This provides an intrinsic thermal emittance of 6.5 μm, as found from the equation [8]

$$\varepsilon = \frac{2r_k}{\beta\gamma}\sqrt{\frac{k_B T}{mc^2}}\,, \tag{24}$$

where k_B is the Boltzmann constant and mc^2 is the rest mass energy of the electron. For this example, we choose to focus the beam to a waist of radius 5 mm located 25 cm downstream from the gun exit. Immediately downstream of the thin lens, Eq. (1) predicts a radius of 9.0 mm, while Eq. (2) predicts a divergence of -0.026. The emittance-limited waist radius is then predicted by Eq. (7) to be 0.25 mm, which is much smaller than the desired waist, confirming that our assumption of a cold beam is satisfied in this case. Choosing a lens strength of 8 m^{-1}, our model then calls for an electron gun with linear parameters of a_0 = 0.0050 m, a_1 = 0.0040 mA^{-1}, b_0 = 0.04, and b_1 = 0.00613 A^{-1}, calculated from Eqs. (18) - (21).

To assess the usefulness of our approach, we now gradually relax our previous assumptions, with the comparisons of beam envelope shown in Figure 9 and the comparisons of trace space configuration shown in Figure 10. Envelopes and trace space information are shown for beam slices with 100%, 80%, 60%, 40%, 20%, and 0% of the peak current, and trace space plots are shown for the beam configuration just upstream of the lens, at the intended location of the waist, and at a distance of $2z_w$ from the gun.

The first row in each figure shows the idealized case, using values calculated from Eq. (1), modified by taking $z \to z_w - z$ upstream of the waist and $z \to z - z_w$ downstream of the waist. As intended, all slices of the beam converge to the desired waist at the desired location.

B. Comparison to Envelope Equation

The first question to be answered is, what error is introduced by our use of a simple model for beam transport? To answer this, we calculated the beam envelopes using the envelope equation, Eq. (8), using the desired initial conditions upstream of the lens, Eqs. (9) and (10) and assuming zero emittance. To replicate a thin lens, a lens length of 0.5 mm was used. The results are shown in the second row of Figures 9 and 10.

C. Desired and Interpolated Initial Conditions

We next switch from using the desired initial conditions calculated using Eqs. (9) and (10), to the interpolated initial conditions calculated from Eqs. (14) and (15) using the linear parameters calculated using Eqs. (18) - (21). For clarity, we also show these initial conditions in red in Figure 10. As described above, the zero current and peak current slices overlap perfectly, but there is an imperfect match of the remaining slices. This results in only minor changes.

D. Emittance

The next row in the figures is identical, except that the cathode thermal emittance value calculated above is now used for the beam emittance. Again, this results in only minor changes.

E. Thick Lens

Finally, we relax our assumption of a thin lens, and instead use a lens which is 3 cm in length; the thick blue line in this figure indicates the shape of the function $k_0(z)$. Now we see a more significant change, with the beam waists for the different current slices being thrown at different locations. Also shown on this plot, in green, is the trace space configuration of the

beam calculated using the thicker lens at the location of the waist in the peak-current slice, rather than the desired location of the beam waist, showing the minor difference in trace space configuration.

Note that in all of these cases, the beam configuration in trace space at the desired location of the waist was well behaved, without formation of any significant low-current secondary distribution due to suboptimal focusing as is sometimes observed [35]. We therefore conclude that the technique discussed here is a reasonable approximate approach to specify electron gun outputs for matching into a focusing lens for focusing to a waist.

IV. Implications for Electron Gun Design

While the approach described above provides a technique to estimate the required electron gun parameters needed to compensate for space charge effects in the lens and drift system considered here, it does not establish whether those parameters can actually be achieved in any electron gun. In this section, we discuss the requirements imposed on electron guns by this model, with an emphasis on understanding the electron gun design elements governing the transverse-longitudinal correlation generated by the gun.

First, as mentioned above, the transport system shown in Figure 1 requires that the electron beam arriving at the lens be diverging, even in the zero-current limit, and that the lens strength be adjusted to eliminate that zero-current divergence. This must be the case because the zero-current slice of the beam has no appreciable space charge to counteract any initial radial convergence as it propagates from the lens to the desired waist location. This requirement eliminates traditional Pierce guns [28], which are designed to produce zero-divergence beams at full current and therefore provide a converging beam in the zero current limit.

This suggests the use of a Pierce-like gun using a larger focusing electrode angle, such as the 100° angle gun shown in Figure 6, which will provide diverging beams at all values of beam current. However, a comparison of the trace space distribution produced by this gun (Figure 6) with the desired trace space configuration (Figure 4) shows an important difference: the zero-current point (B) and the peak-current point (A) fall on the lower bounding line for the 100° angle gun, while they fall on the upper bounding line for the desired trace space configuration. To understand the source of this discrepancy, compare Eqs. (11) and (16). Each equation consists of two terms. The first term is linear in r , with the coefficient determining the slope of the bounding line along which points A and B fall. The second term determines where that bounding line crosses the r' -axis. If this second term is positive, then A and B must fall along the upper bounding line, which intercepts the r' -axis at a positive value of r' ; if the second term is negative, then A and B must fall along the lower bounding line, which intercepts the r' -axis at a negative value of r' . Eq. (11) shows that for the desired distribution, the intercept scales with the ratio of beam waist radius and waist location -- $1.617 r_w / z_w$ -- and therefore *must* be positive, putting A and B on the upper bounding line. This imposes an additional requirement on the electron gun: in order to match the desired trace space configuration, any potential gun must generate a beam with linear parameters chosen so that its peak and zero-current slices also fall along the upper bounding line, and so the second term in Eq. (16) -- $b_0 - a_0 b_1 / a_1$ -- must also be positive. However, this quantity is negative for the 100° angle gun shown in Figure 6; in fact, it is negative for *all* the electron gun configurations considered by us in Refs. [3] and [4], as well as the 100 kV, 300 kV, and 500 kV apertured configurations in the new TRAK simulations. What design features of these guns cause this quantity to be negative?

A clue to this lies in Figure 6 itself. Note that in both the peak current case (A) and the zero-current case (B), the beam envelope is virtually linear with position except for the region closest to the source. This is the location where the beam density is highest, and therefore where the radial space charge will be strongest, not only because in a diverging gun the beam radius will be smallest here, but also because of the beam acceleration which leads to a density scaling with $z^{-2/3}$ even in the ideal, divergence-free case assumed by the Child-Langmuir law [36]. Additionally, the electrode shaping which generates the time-independent focusing or defocusing effect in the gun was only employed on the cathode side. The apparent result of these effects was to cause the majority of the focusing or defocusing action to occur near the cathode, with the trajectories far from the cathode being roughly linear in position.

Now, for the sake of argument, let us assume that *all* of the focusing or defocusing effect occurred at the cathode surface, and that the electron beam envelope was linear in position for the rest of its travel across the anode-cathode gap, as shown in the portion of Figure 11 between the cathode plane and anode plane. In that case, for zero current, $I \to 0$, the radius would be

$$a_0 = r_k + b_0 d_{AK}\,, \tag{25}$$

where r_k is the cathode radius and d_{AK} is the anode-cathode distance. Similarly, for peak current, $I \to I_{\max}$, and radius would be

$$a_0 + a_1 I_{\max} = r_k + \left(b_0 + b_1 I_{\max}\right) d_{AK}\,. \tag{26}$$

In this case, the second term in Eq. (16) becomes

$$b_0 - \frac{a_0 b_1}{a_1} = -\frac{r_k}{d_{AK}}\,, \tag{27}$$

which is always negative, and therefore requires the peak-current and zero-current points A and B to fall along the lower bounding line -- as, in fact, they do. This scaling holds remarkably well for our simulation data given its simplicity (Figure 12).

We therefore conclude that the requirements developed in Section II are unlikely to be satisfied by an electron gun in which the majority of the defocusing action occurs near the cathode, and consider whether shifting some of the defocusing to the anode plane by addition of an electrostatic lens can achieve the required initial configuration. We return to Figure 11, but now assume a thin lens in the anode plane followed by a drift space which is short enough that space charge can be neglected. The lens is assumed to provide a change in divergence equal to

$$\Delta b = \frac{1}{f}\left(a_0 + a_1 I\right). \tag{28}$$

The beam divergence at the image plane is then

$$B_0 + B_1 I = b_0 + b_1 I + \frac{1}{f}\left(a_0 + a_1 I\right), \tag{29}$$

while the beam radius at the image plane is

$$A_0 + A_1 I = \left(a_0 + a_1 I\right) + d_1\left(B_0 + B_1 I\right), \tag{30}$$

where the variables are capitalized to distinguish the linear parameters in the image plane from those in the anode plane. This implies

$$B_0 = b_0 + \frac{1}{f}\left(r_k + b_0 d_{AK}\right), \tag{31}$$

$$B_1 = b_1\left(1 + \frac{d_{AK}}{f}\right), \tag{32}$$

$$A_0 = r_k + b_0 d_{AK} + d_1 b_0 + \frac{d_1}{f}\left(r_k + b_0 d_{AK}\right), \tag{33}$$

and

$$A_1 = b_1\left(d_{AK} + d_1 + \frac{d_1 d_{AK}}{f}\right), \tag{34}$$

and therefore

$$B_0 - \frac{A_0 B_1}{A_1} = -\frac{r_k}{d_{AK} + d_1 + \frac{d_1 d_{AK}}{f}}, \tag{35}$$

which reduces to Eq. (27) in the limit $d_1 \to 0$, as expected. If the lens is defocusing, $1/f < 0$, which provides the opportunity for Eq. (35) to become positive, therefore allowing the trace space configuration shown in Figure 4. Identifying Eq. (35) with the second term in Eq. (11) gives an expression for the required lens strength:

$$\frac{1}{f} = -\left(\frac{r_k z_w}{1.617 r_w d_1 d_{AK}} + \frac{1}{d_1} + \frac{1}{d_{AK}}\right). \tag{36}$$

Assume the following typical values: cathode radius of 0.5 mm, drift distance of 5 cm between the electrostatic lens and the solenoid, waist radius of 1 cm, distance to waist of 10 cm, anode-cathode gap of 5 cm. This gives a required lens strength of -52.3 m^{-1}.

Finally, we use Eq. (36) to ask whether the aperture lens occurring naturally at the exit of an electron gun in the absence of an anode grid provides sufficient defocusing. The strength of that lens will be [8]:

$$\frac{1}{f} = -\frac{V'}{4V_{AK}} \approx -\frac{1}{4d_{AK}}, \tag{37}$$

assuming $V' = V_{AK}/d_{AK}$, which is clearly smaller than the quantity in Eq. (36). Additional defocusing is therefore required to achieve the desired beam configuration.

V. Summary

In this paper, we considered the requirements for a current-modulated, space charged dominated electron beam to be focused to a waist with radius and location independent of slice current in a simple injector consisting of an electron gun, lens, and drift section. Each of the three elements was initially treated using phenomenological or analytic approximations, and the assumptions and range of applicability of these approximations was studied. The approximation introducing the most error in the tested cases was the use of a thin lens model for the solenoid. To achieve a waist which was independent of current, the transverse-longitudinal correlation imposed on the beam by the electron gun must be tailored to compensate for the transverse-longitudinal correlation imposed on the beam during its travel through the lens and drift section, effectively serving in a "feed forward" role. This required initial correlation was specified in terms of the other system properties using a linear parameterization of radius and divergence on slice current, first developed for low energy electron guns using anode grids, but shown here to also provide a reasonable description of the beams generated in apertured electron guns at voltages up to 500 kV. This parameterization was used as a tool to investigate the impact of an electron gun's design on its ability to achieve the required initial transverse-longitudinal correlation. It was found that neither defocusing occurring purely at the cathode nor the defocusing associated with aperture lensing were sufficient, but that the addition of extra electrostatic defocusing at the anode could achieve the desired effects.

ACKNOWLEDGEMENTS

Portions of this work were performed under the auspices of the U.S. Department of Energy by Lawrence Livermore National Laboratory under Contract DE-AC52-07NA27344.

REFERENCES

[1] B.E. Carlsten, Nuclear Instruments and Methods A **285**, 313-319 (1989).

[2] L. Serafini and J.B. Rosenzweig, Physical Review E **55,** 7565-7590 (1997).

[3] J.R. Harris, J.W. Lewellen, and B.R. Poole, Journal of Applied Physics **112**, 023304 (2012).

[4] J.R. Harris, J.W. Lewellen, and B.R. Poole, Journal of Applied Physics **114**, 063304 (2013).

[5] D. Shiffler, et al., IEEE Transactions on Plasma Science **38**, 1462-1465 (2010).

[6] G.J. Caporaso, et al., "Status of the Dielectric Wall Accelerator," in Proceedings of the 2009 Particle Accelerator Conference, Vancouver, Canada, 4-8 May 2009.

[7] B.R. Poole and J.R. Harris, Physics of Plasmas **20**, 043108 (2013).

[8] M. Reiser, *Theory and Design of Charged Particle Beams*, Wiley: New York (2008).

[9] J.R. Harris and J.W. Lewellen, Physics of Plasmas **17**, 043101 (2010).

[10] J.R. Harris and P.G. O'Shea, IEEE Transactions on Electron Devices **53**, 2824-2829 (2006).

[11] H. Ishizuka, et al., Nuclear Instruments and Methods A **445**, 276-280 (2000).

[12] I.T. Han, et al., Applied Physics Letters **81**, 2070 (2002).

[13] D.W. Feldman, et al., "Combined Thermionic and Photoelectric Emission from Dispenser Cathodes," in Proceedings of the 2001 Particle Accelerator Conference, Chicago, IL.

[14] R.A. Kishek, et al., Nuclear Instruments and Methods A **544**, 179-186 (2005).

[15] S.E. Sampayan, S.H. Gurbaxani, and M.T. Buttram, Journal of Applied Physics **68**, 2058 (1990).

[16] J.R. Harris, A.I. Yilmaz, and D.D. Snyder, IEEE Transactions on Plasma Science **41** 3624-3633 (2013).

[17] J.R. Harris, Journal of Applied Physics **115**, 193302 (2014).

[18] J.R. Harris, et al., IEEE Transactions on Plasma Science **37** 1069-1077 (2009).

[19] J.P. Edelen, et al., IEEE Transactions on Nuclear Science **61**, 830-836 (2014).

[20] J.R. Harris, et al., Physical Review E **76**, 026402 (2007).

[21] B.R. Poole, et al., "Space Charge Waves in Mismatched Beams," in Proceedings of the 2009 Particle Accelerator Conference, Vancouver, Canada, 4-8 May 2009.

[22] H. Spachmann and U. Becker, Nuclear Instruments and Methods A **558** 50-53 (2006).

[23] M. Borland, "Summary of Equations and Methods used in SPIFFE," APS/ IN/LINAC/92-2, 29 June 1992.

[24] S. Humphries, Journal of Computational Physics **125**, 488-497 (1996).

[25] R.D. Scarpetti, R.W. Kuenning, and K.C. Wong, IEEE Transactions on Nuclear Science **28**, 3430-3432 (1981).

[26] J.G. Wang, et al., IEEE Transactions on Electron Devices **37**, 2622-2628 (1990).

[27] J.R. Harris and P.G. O'Shea, Journal of Applied Physics **103**, 113301 (2008).

[28] J.R. Pierce, Journal of Applied Physics **11,** 548 (1940).

[29] H. Craig Miller, IEEE Transactions on Electrical Insulation **24**, 765 (1989).

[30] J.R. Harris, et al., Applied Physics Letters **91**, 121504 (2007).

[31] J.R. Harris, et al., Applied Physics Letters **93**, 241502 (2008).

[32] P. Evtushenko, F.E. Hannon, and C. Hernandez-Garcia, "Electrostatic Modeling of the Jefferson Laboratory Inverted Ceramic Gun," in Proceedings of the 2010 International Particle Accelerator Conference, Kyoto, Japan.

[33] The sudden jump exhibited by the last point in these graphs was also seen at the onset of space charge limited operation in the simulations reported in Ref. [3].

[34] This implies $r'(I=0)=0$ on leaving the lens. If $r'(I=0)<0$, the zero-current slice would reach a waist which would be governed by emittance, which is outside the scope of our assumptions.

[35] D. Filippetto, et al., Nuclear Instruments and Methods A **605** 215-223 (2009).

[36] K.R. Spangenberg, *Vacuum Tubes,* McGraw-Hill: New York, 1948. p. 172.

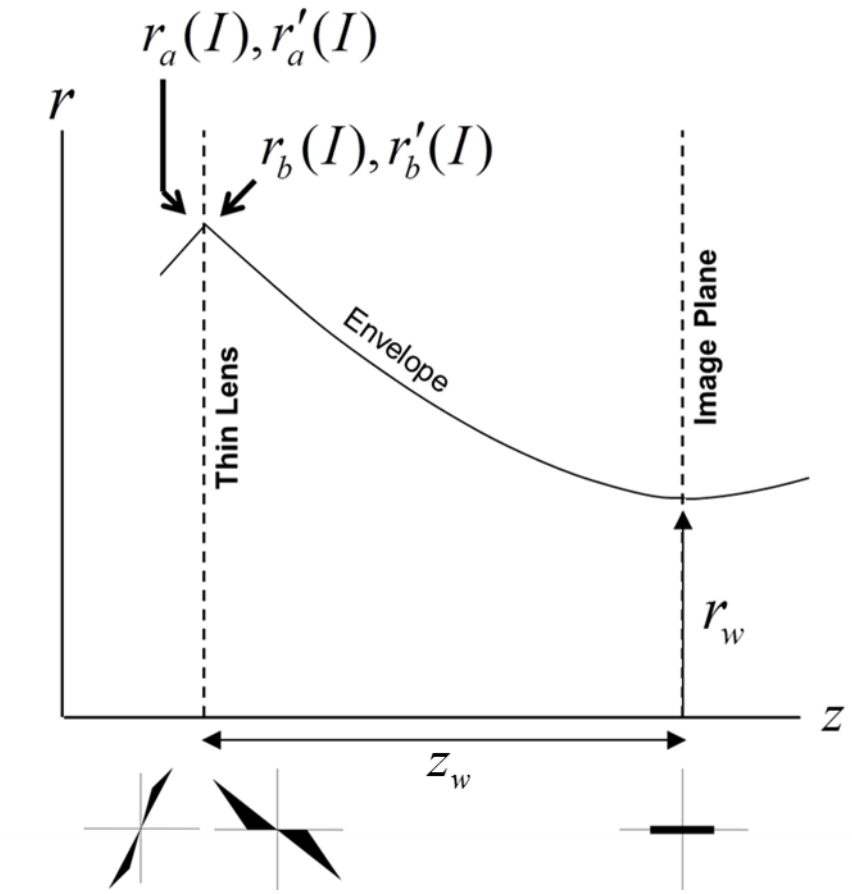

Figure 1. System geometry. A current-modulated DC electron gun is assumed to be immediately upstream of the thin lens. Insets at bottom indicate the beam's desired configuration in trace space before the lens (corresponding to Figure 4), after the lens (corresponding to Figure 2), and at the waist.

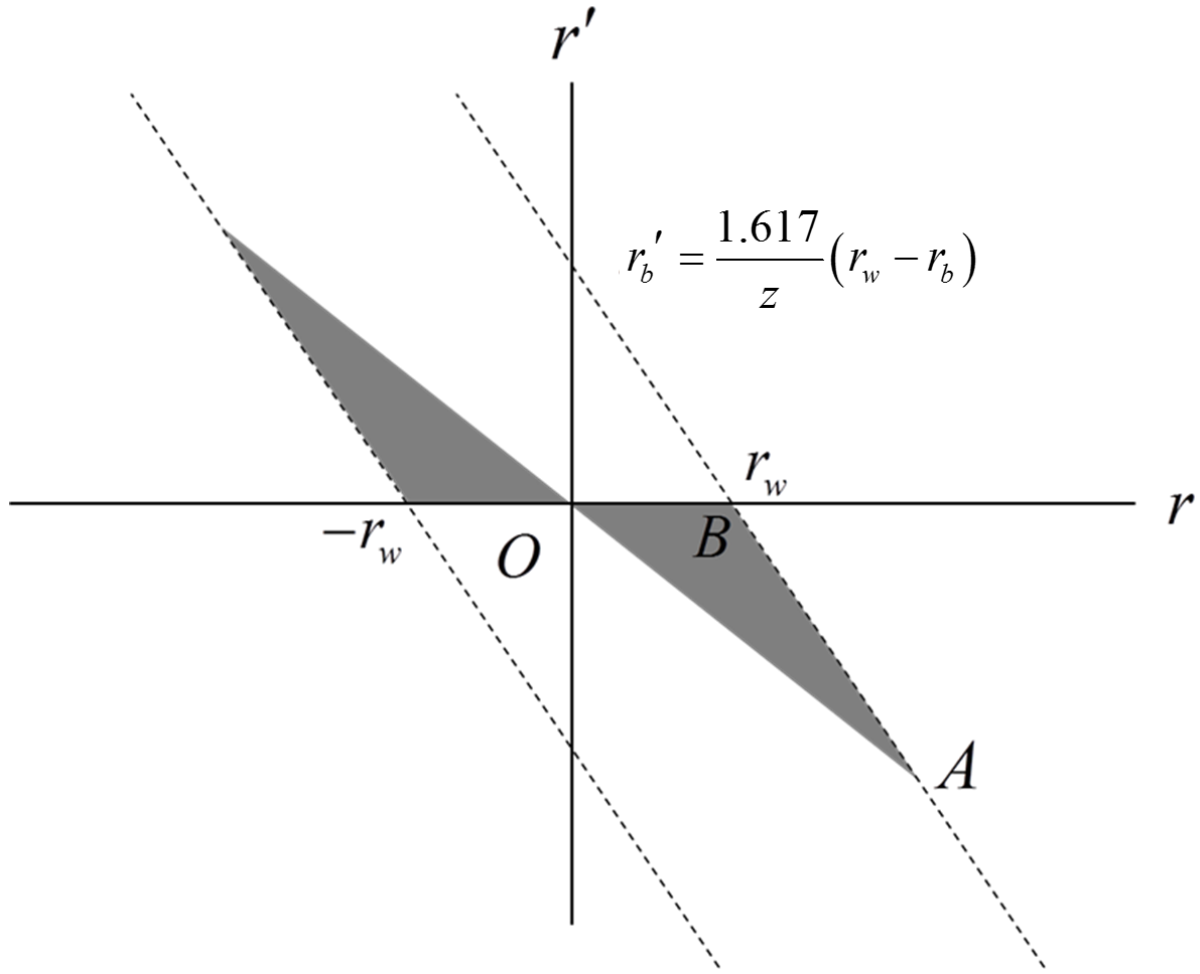

Figure 2. Trace space construction for a beam compressing to a waist of radius r_w. In the second quadrant, this line is populated between point A, corresponding to the peak-current slice in the beam and having coordinates given by Eq. (4); and point B, corresponding to the zero-current slices.

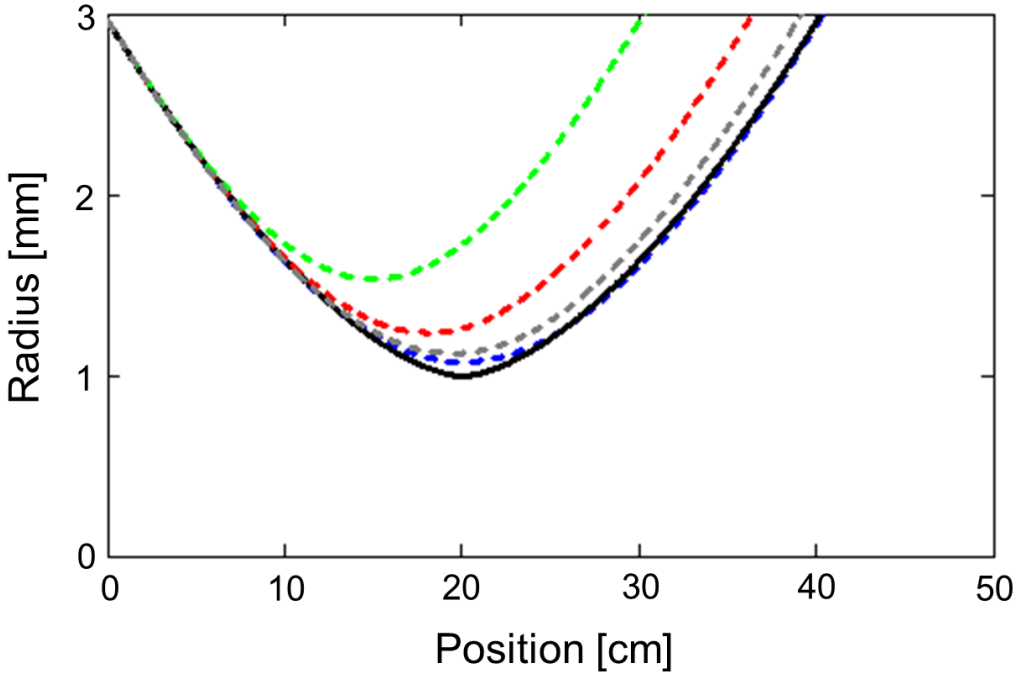

Figure 3. Beam envelopes for a 50 keV, 100 mA beam with initial radius of 2.969 mm and initial divergence of -0.016, calculated using Eq. (1) (black) and from Eq. (8) with emittance values of zero (blue), 4.02 μm (gray), 8.12 μm (red), and 17.00 μm (green).

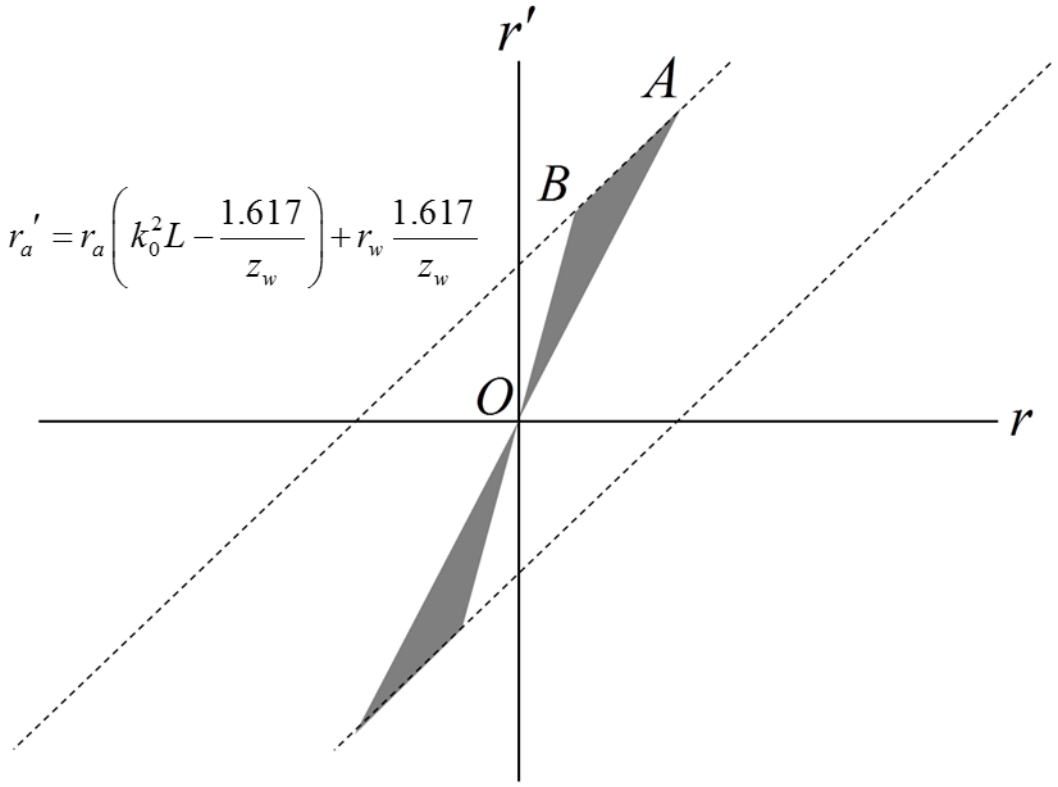

Figure 4. Required trace space configuration just upstream of the lens, showing the orientation of the zero current slice (point B, location given by Eq. (12)) and peak current slice (point A, location given by Eq. (13)).

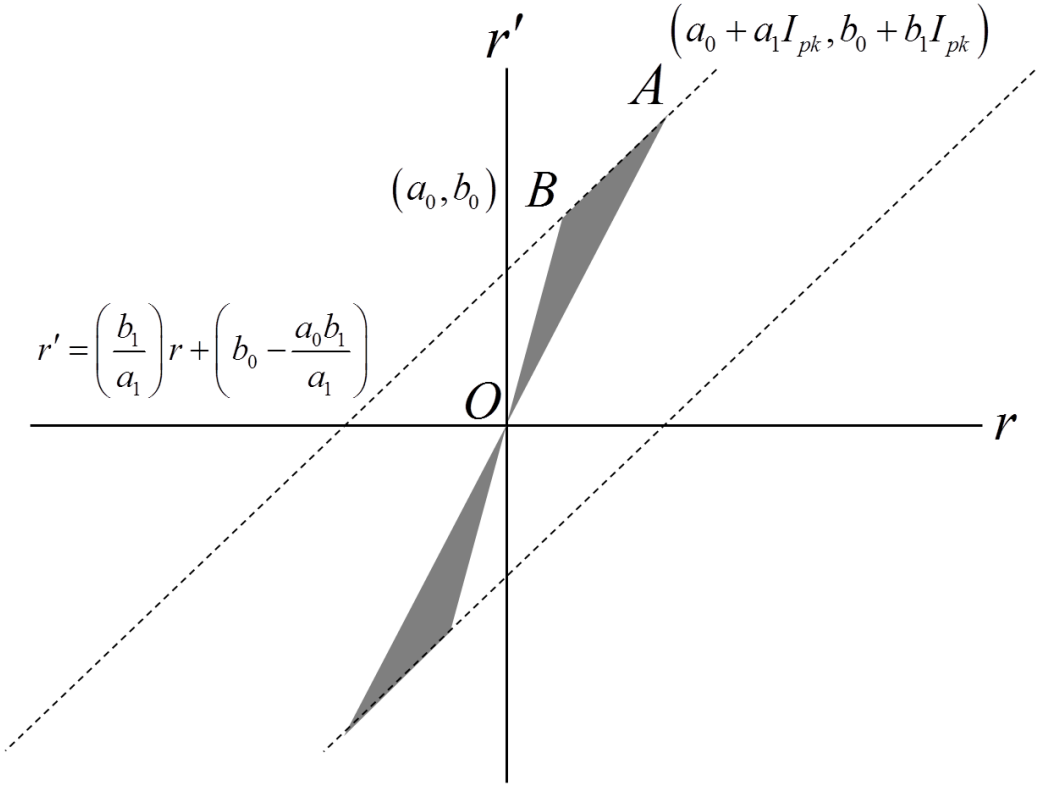

Figure 5. Trace space diagram for a beam produced with initial linear dependence of radius and divergence on beam current, showing the orientation of the zero-current slice (point B, with location $\left(a_0, b_0\right)$) and peak current slice (point A, with location $\left(a_0 + a_1 I_{pk}, b_0 + b_1 I_{pk}\right)$).

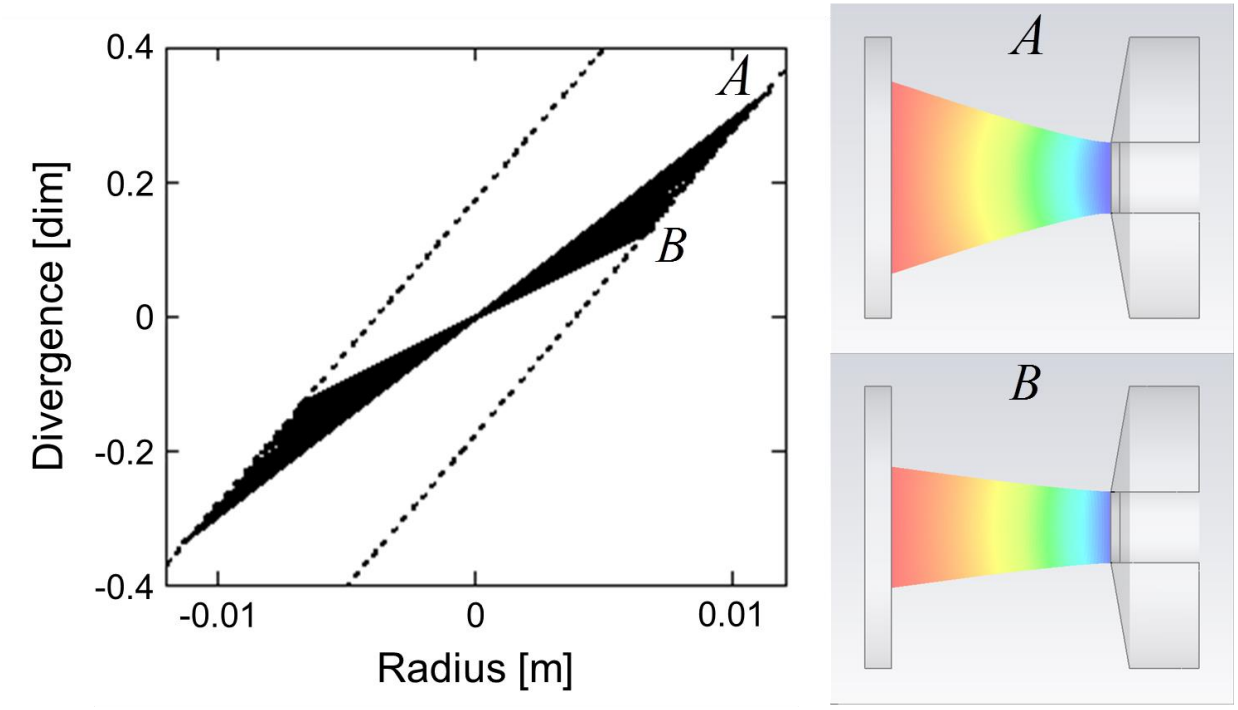

Figure 6. Simulations of a simplified 10 keV electron gun using CST Particle Studio. Anode-cathode spacing is 25 mm, and the focusing electrode angle is 100° with respect to the gun axis. The trace space figure at left shows an overlay of the beam orientation at the anode for 17 simulation runs at currents varying between 0.1 mA (B) and 1.33 A (A , the space charge limit); the corresponding simulated beam trajectories are shown at right, with particle energy denoted by color. The dotted lines in the trace space figure are computed from Eq. (16) using the linear parameters obtained for this configuration (a_0 = 0.00672 m, a_1 =0.00335 mA^{-1}, b_0 =0.130, b_1 =0.152A^{-1}), showing excellent agreement between the simulation results and the linear parameterization.

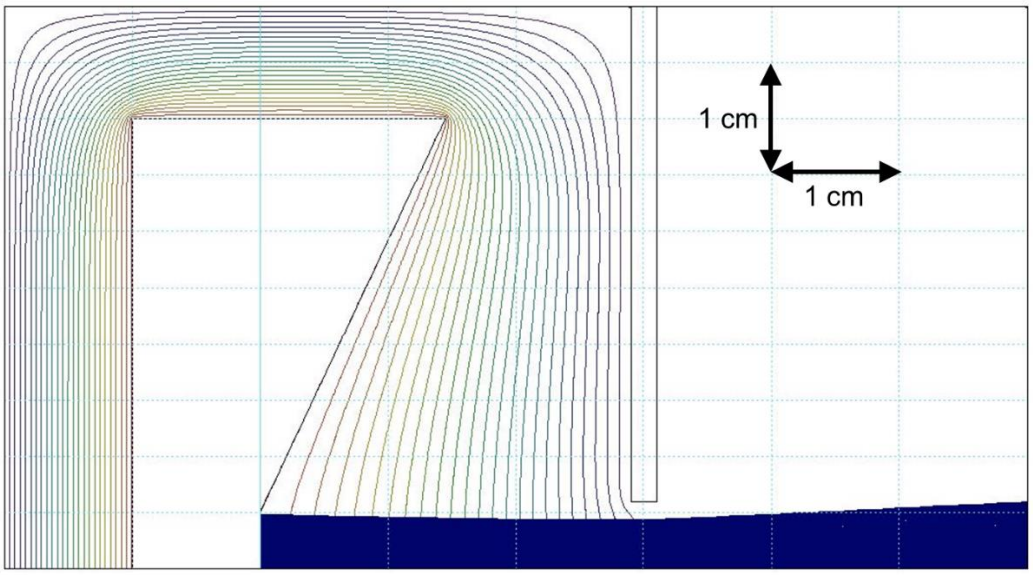

Figure 7. TRAK simulation of a simplified apertured electron gun, showing equipotential lines and typical electron trajectories for the 300 kV case, operating at a space charge limited current of 31.4 A. Simulations were performed with anode-cathode voltages of 100 kV, 300 kV, and 500 kV. The focusing electrode angle was 67.5°, cathode radius was 0.5 cm, anode aperture radius was 0.6 cm, and anode-cathode distance was 3 cm. One diagnostics plane was placed in the plane of the aperture, and three more were placed 0.6 cm, 1.2 cm, and 1.8 cm downstream of the aperture plane.

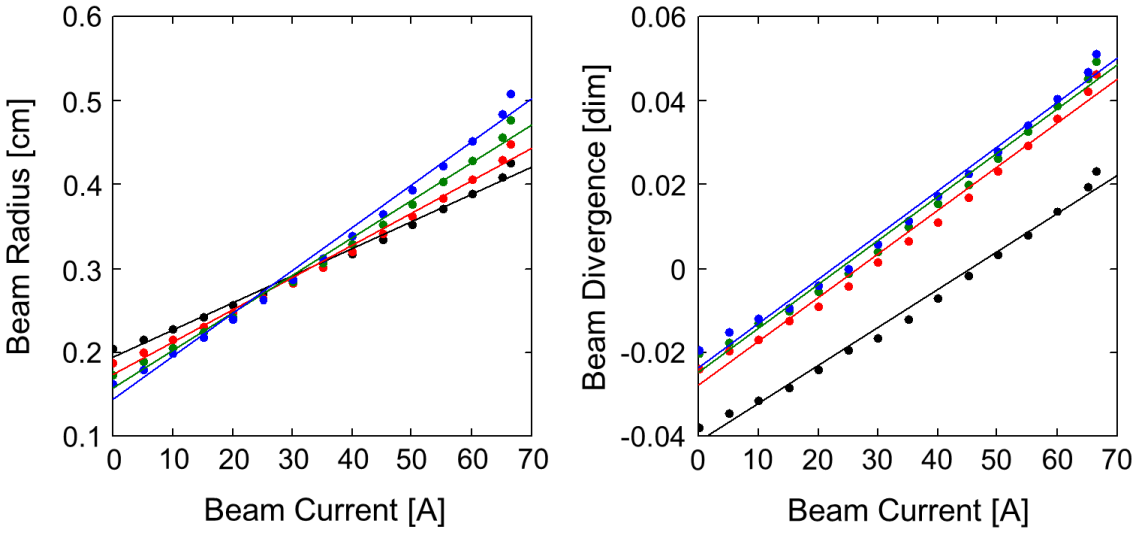

Figure 8. Beam radius and divergence for the 500 kV gun using edge radius and divergence data extracted directly from the phase space data generated by the simulation, compared to linear fitting functions. Data extracted at the anode plane (black), and at 0.6 cm (red), 1.2 cm (green), and 1.8 cm (blue) downstream from the anode plane.

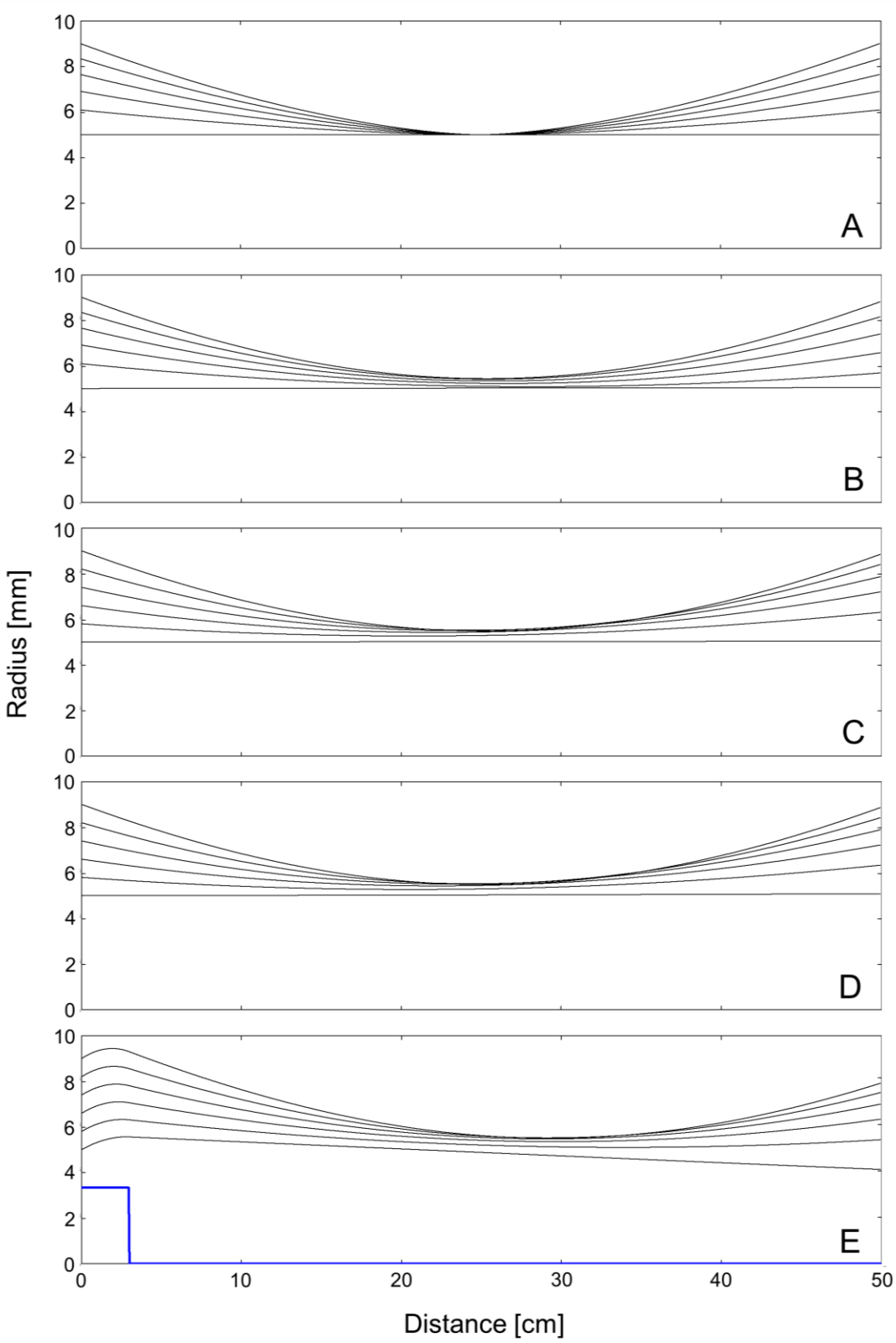

Figure 9. Beam envelopes for example case. Letters correspond to subsections in Section III.

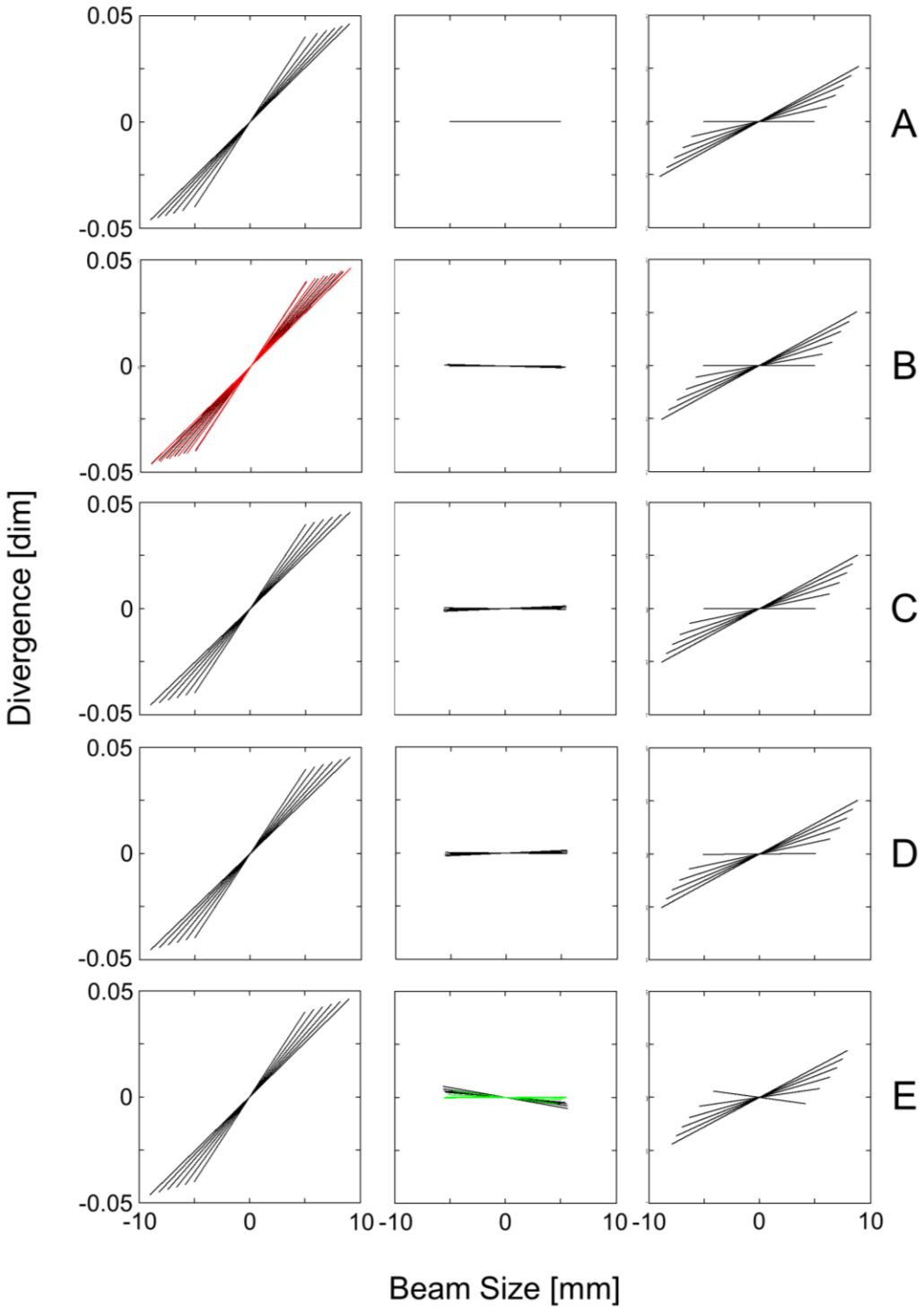

Figure 10. Trace space configurations for beam at start plane (left), nominal waist location (center), and twice the nominal waist location (right). Letters correspond to subsections in Section III.

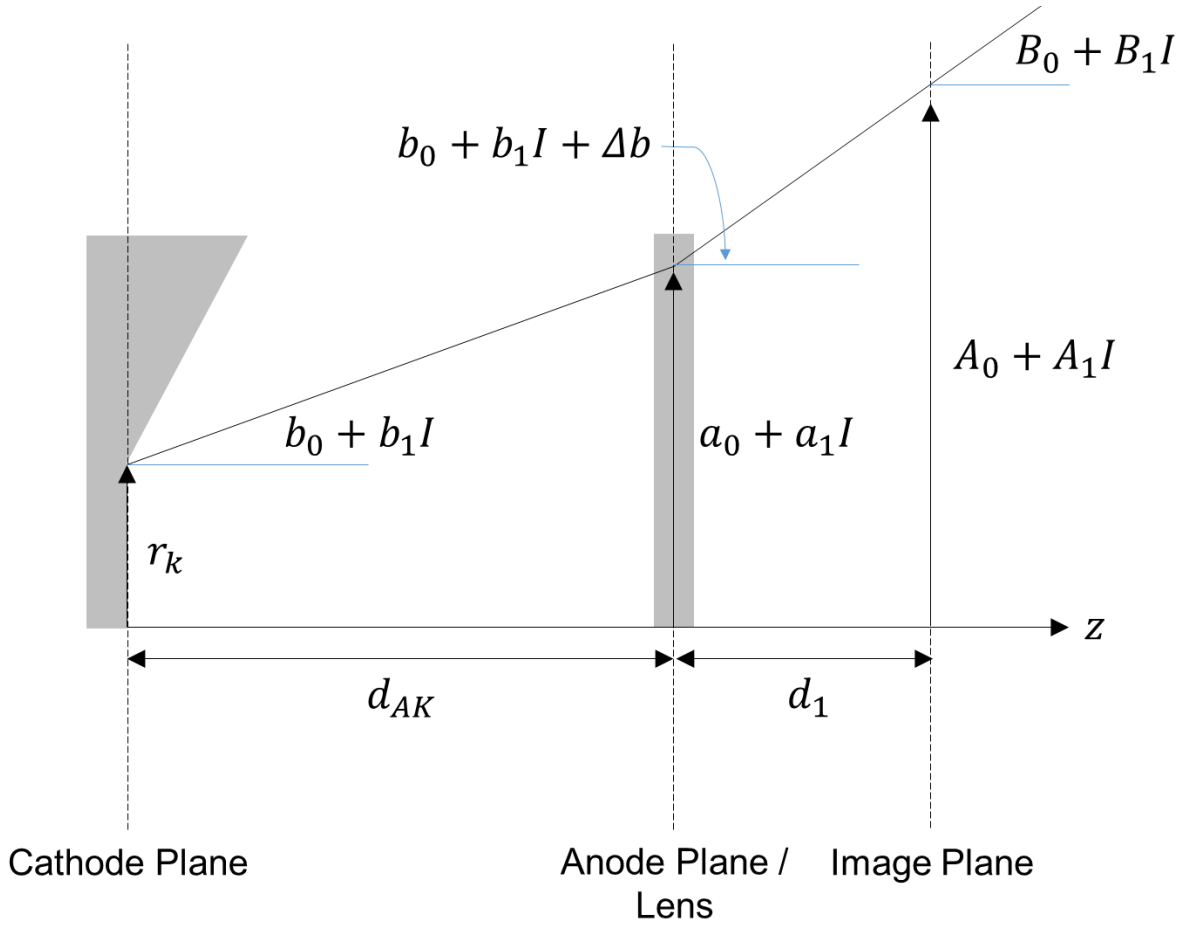

Figure 11. Configuration for beam transport in diode with straight line paths.

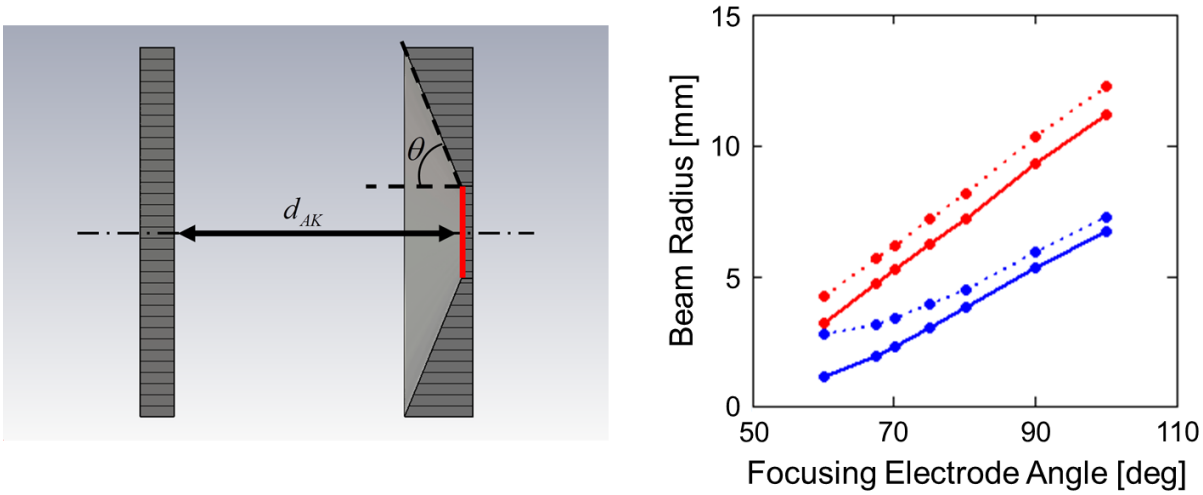

Figure 12. (Left) Simulated electron gun configuration, with anode-cathode voltage of 10 kV, anode-cathode distance d_{AK} of 25 mm, cathode radius r_k of 4 mm, and variable focusing electrode angle θ. (Right) Comparison of simulation results with model assuming all focusing action occurs at the cathode surface, showing beam radius at the anode as a function of focusing electrode angle at zero current (blue) and at the space charge limit (red). The solid line indicates actual simulation results, while the dotted line indicates predictions from Eq. (25) and Eq. (26) using values of a_n and b_n tabulated in Ref. [4].